



HAL
open science

Effect of simultaneous Cu and Nb doping Bi₄V₂O₁₁ on structural and electrical properties of Bi₄V_{2-*x*}Cu_{*x*}/2Nb_{*x*}/2O_{11-3*x*}/4

Wafaa Mhaira, Abdelmajid Agnaou, Rachida Essalim, Andrea Turino, Fabrice Mauvy, Maati Alga, Mohamed Zamama, Abdelaziz Ammar

► **To cite this version:**

Wafaa Mhaira, Abdelmajid Agnaou, Rachida Essalim, Andrea Turino, Fabrice Mauvy, et al.. Effect of simultaneous Cu and Nb doping Bi₄V₂O₁₁ on structural and electrical properties of Bi₄V_{2-*x*}Cu_{*x*}/2Nb_{*x*}/2O_{11-3*x*}/4. *Journal of Solid State Chemistry*, 2023, 320, 123878 (7 p.). 10.1016/j.jssc.2023.123878 . hal-04018520

HAL Id: hal-04018520

<https://hal.science/hal-04018520>

Submitted on 7 Mar 2023

HAL is a multi-disciplinary open access archive for the deposit and dissemination of scientific research documents, whether they are published or not. The documents may come from teaching and research institutions in France or abroad, or from public or private research centers.

L'archive ouverte pluridisciplinaire **HAL**, est destinée au dépôt et à la diffusion de documents scientifiques de niveau recherche, publiés ou non, émanant des établissements d'enseignement et de recherche français ou étrangers, des laboratoires publics ou privés.

Effect of simultaneous Cu and Nb doping $\text{Bi}_4\text{V}_2\text{O}_{11}$ on structural and electrical properties of $\text{Bi}_4\text{V}_{2-x}\text{Cu}_{x/2}\text{Nb}_{x/2}\text{O}_{11-3x/4}$

W. Mhaira^(a), A. Agnaou^(a), R. Essalim^(a), A. Turino^(b,c), F. Mauvy^(b), M. Alga^(a), M. Zamama^(a) and A. Ammar^(a).

^(a) Laboratoire des Sciences des Matériaux et Optimisation des Procédés (SCIMATOP), Université Cady Ayyad, Faculté des Sciences Semlalia, Av. Prince Moulay Abdellah, B.P. 2390, Marrakech, Morocco.

^(b) University of Bordeaux, CNRS, Bordeaux INP, ICMCB, UMR 5026, 33600 Pessac, France

^(c) Department of Chemical Sciences - University of Padova - Via Marzolo, 1 35131 Padova, Italy

Abstract

BiMeVO_x compounds $\text{Bi}_4\text{V}_{2-x}\text{Cu}_{x/2}\text{Nb}_{x/2}\text{O}_{11-3x/4}$ doubly substituted solid solution, with identical compositions of Cu^{2+} and Nb^{5+} ions, show an area of existence from $x = 0$ to 0.5. X-ray diffraction measurements and thermal analysis have shown that, depending on the composition, the three main $\text{Bi}_4\text{V}_2\text{O}_{11}$ polymorphs α , β and (γ/γ') are observed at room temperature. The evolution of the electrical conductivity with the rate of substitution has been investigated by electrochemical impedance spectroscopy (EIS) in the temperature range 120-720°C. The highest values of conductivity are observed for samples with $x = 0.2$. Scanning electron microscopy (SEM) shows an important grain growth and the presence of micro-cracks in the ceramics with $x = 0.5$ composition.

Keywords: Aurivillius phases, $\text{Bi}_4\text{V}_2\text{O}_{11}$, BIMEVOX materials, ionic conductivity.

1. Introduction

Since 1949, when the so-called Aurivillius phases were firstly reported in the literature [1], many works have been dedicated to this lamellar family. Dozens of them had focalized on their remarkable ferroelectric properties induced, mostly, by the lone pair of electrons Bi 6s² which plays an important role in the behavior of both structural and electrical properties [2–5]. The general formula of the Aurivillius phases can be written as $(\text{Bi}_2\text{O}_2)^{2+}(\text{A}_{n-1}\text{B}_n\text{O}_{3n+1})^{2-}$ where $(\text{Bi}_2\text{O}_2)^{2+}$ has a pyramidal form with a square base formed by oxygen and bismuth occupies their top. The $(\text{A}_{n-1}\text{B}_n\text{O}_{3n+1})^{2-}$ structural group is constituted by n perovskite layers.

After thirty-six years, a new member of Aurivillius phases with $n = 1$, in the Bi-V-O system was identified in 1985 by Bush et al [6]. The formula of this compound is $\text{Bi}_4\text{V}_2\text{O}_{11}$. Its structure consists of an intergrowth of fluorite-like layers $(\text{Bi}_2\text{O}_2)^{2+}$ and perovskite-like sheets $(\text{VO}_{3.5}\square_{0.5})^{2-}$, intrinsically oxygen-deficient [7,8]. This oxide undergoes series of phase transitions, with temperature, from monoclinic α - $\text{Bi}_4\text{V}_2\text{O}_{11}$ form, stable at room temperature, to an orthorhombic structure β - $\text{Bi}_4\text{V}_2\text{O}_{11}$ at 450°C and then to tetragonal γ - $\text{Bi}_4\text{V}_2\text{O}_{11}$, beyond 580 °C. The last form exhibits high degree of disorder which lead to an important oxygen ionic conductivity at a relatively low temperature (0.2 S.cm⁻¹ at 600°C [9]).

The X-ray diffraction pattern of the γ form given by Abraham et al. [9] was exactly the same as the pattern of our product. This form is characterized by a random oxide ion vacancies distribution, which seems to be responsible for the excellent ionic conductivity (0.2 S.cm^{-1} at 600°C). Moreover, it was demonstrated later that there is another high form, γ' , with a tetragonal symmetry, but less conductive than the γ phase. The loose of the conductivity performances is due to the establishment of partial oxygen vacancy order [10].

Because of this new remarkable attractive property of this class of Aurivillius phases, the work has been refocused on the ionic conductivity instead of the ferroelectricity. Hence, numerous solid solutions had been prepared by substituting vanadium (V^{5+}) by other metallic cations. These solid solutions constitute a family of compounds known by the acronym BiMeVOX (Me= Co, Cu, Mn, ...) [11–16]. Generally, the α , β and γ forms are progressively stabilized by increasing the substitution rate.

According to dozens of works published in the literature, it can be concluded that the solid solution limits depend generally on the valence and the preferred coordination geometry of the substituent cation [17–19]. The best conductivity is always obtained when close to 10% of V^{5+} in $\text{Bi}_4\text{V}_2\text{O}_{11}$, has been substituted by 10% of the metal independently of its oxidation state and its nature [10,14].

Also, many double substitutions at the V-site or Bi/V have been reported in the literature [10,20–23]. Some studies have been focused on $\text{Bi}_4\text{V}_{1.8}\text{M}_{0.1}\text{M}'_{0.1}\text{O}_{11-d}$ solid solutions (where M is a divalent element and M' is tetra or pentavalent cations) with the aim of an enhancement of the ionic conductivity by some “synergic effect” [12,20]. However, the effect of the double substitution on the electrical properties is diverse. If Vannier et al. [24] have not observed any improvement in the oxide anion conductivity in the case of materials with M and M' = Cu^{2+} , Ni^{2+} and Zn^{2+} , Paydar, in contrast, has reported an increase of the ionic conductivity of the compound with M = Cu^{2+} and M' = Ti^{4+} [20].

In 2005, we have reported the result of a study on materials obtained by double substitution of V^{5+} by copper and niobium in the limit of 10%, and a slightly improved electrical conductivity have been demonstrated. Niobium and copper have been selected owing to the large conductivity at relatively moderate temperature of $\text{Bi}_4\text{V}_{1.8}\text{Nb}_{0.2}\text{O}_{11}$ ($\sigma \approx 2.5 \cdot 10^{-2} \text{ S.cm}^{-1}$ at 550°C) [25] and of $\text{Bi}_4\text{V}_{1.8}\text{Cu}_{0.2}\text{O}_{10.7}$ ($\sigma \approx 4 \cdot 10^{-2} \text{ S.cm}^{-1}$ at 600°C) [26].

Therefore, the aim of the present work is to show the results of the extended study to the whole composition domain of the solid solution $\text{Bi}_4\text{V}_{2-x}\text{Cu}_{x/2}\text{Nb}_{x/2}\text{O}_{11-3x/4}$ with $0.1 \leq x \leq 0.5$.

2. Experimental

Different compositions of $\text{Bi}_4\text{V}_{2-x}\text{Cu}_{x/2}\text{Nb}_{x/2}\text{O}_{11-3x/4}$ powder with ($0.0 \leq x \leq 0.5$) were prepared by conventional solid-state reaction of stoichiometric quantities of corresponding oxides Bi_2O_3 (Merck, 99.5%), V_2O_5 (Merck, 99%), CuO (Merck, 98%) and Nb_2O_5 (Merck, 99.9%) previously dried and homogenized. The obtained powders were grounded in an agate mortar for 0.5h, placed in platinum crucibles, heated for 24 hours at 800°C , then slowly cooled to room temperature. Three thermal treatments, with intermediate regrinding, were necessary to obtain pure microcrystalline powders.

The powder samples were characterized by X-ray diffraction using a Rigaku diffractometer, Smart Lab, with $\text{CuK}\alpha$ radiation. The diffractograms were recorded between 10 and $60 (2\theta)$, with a step of $0.02 (2\theta)$. The variation of the unit-cell parameters and the cell volume were obtained using the Fullprof software.

For the ceramic studies, the powder was grounded for 10 min then sieved with $50 \mu\text{m}$ sieves and pressed by uniaxial hand pressing (1 tonne/cm^2) into the form of cylindrical pellets

(8 mm diameter and about 2 mm thickness). The obtained pellets were sintered at 800°C for 10h and slowly cooled to room temperature.

Thermogravimetric analysis (TGA) and differential thermal analysis (DTA) experiments were carried out between 25°C and 750°C on all the samples using a LABSYS Evo TGA 1600 analyzer, at a heating rate of 10°C/min.

The infrared study was carried out on pellets with KBr. The samples were mixed with dried potassium bromide at a sample to KBr quantity mass ratio of 0.01: 0.99. The mixture was then pressed under vacuum. The compacted pellets were analyzed using a Bruker VERTEX 70 FT-IR spectrometer in transmission mode over a frequency range of 400 to 4000 cm⁻¹.

Raman scattering spectra were recorded using a Confotec MR520 spectrometer using samples in pellet form. A laser with ionized argon emitting in the green at wavelength $\lambda = 532$ nm have been implemented.

For scanning electron microscopy observations, the faces of the sintered pellets were polished with SiC paper (1500-5000 grit). Microstructural observations were performed on the polished samples using a scanning electron microscope model VEGA3 LMU. Grain boundaries were revealed using thermal etching at 750°C for 20 min.

Electrical conductivity measurements were performed by Electrochemical Impedance Spectroscopy (EIS) at frequencies ranging from 0.01 to 1 MHz using an AUTOLAB PGSTAT 302. The amplitude of the AC signal applied across the sample was 50 mV. Measurements were performed on sintered pellets (relative density higher than 83%) under steady state conditions. Pellets were first heated to 830°C with a 15 h-dwell time. Pt ink electrodes were deposited on both flat surfaces of the pellets. For each sample, the impedance measurements were recorded under dry air from 120 to 700°C, on isothermal plateau of 60 mn. The experimental impedance spectra were simulated by electrical equivalent circuits composed of resistances and Constant Phase Elements (CPE) associated in parallel. The values of circuit parameters were determined by non-linear least-square fitting using the Z.View software (Scribner Associates).

3. Results and discussion

3.1 XRD characterization and DTA analysis

As a typical example, Figure 1 depicts, the X-ray diffraction pattern of Bi₄V_{2-x}Cu_{x/2}Nb_{x/2}O_{11-3x/4} samples with $x = 0.0, 0.10, 0.15, 0.2, 0.5$ and 0.6 . Three compositional domains can be observed. In domain I ($x \leq 0.10$), the samples are single-phase and the patterns show a doublet close to $2\theta = 55^\circ$ corresponding to hkl reflections (333) and (085) which characterize the α -phase with a monoclinic symmetry and a C2/m space group. Domain II ($0.10 < x < 0.20$), the orthorhombic symmetry of the β -Bi₄V₂O₁₁ form is clearly observed with the presence of 2am super lattice at $2\theta = 24.8^\circ$. In the domain III ($0.2 \leq x \leq 0.5$), the (020) / (200) peaks around $2\theta = 32^\circ$ merge into a singlet (110), indicating the stabilization at room temperature of the tetragonal γ or γ' form space group I4/mmm at room temperature. When $x > 0.5$, a secondary phase Bi₈V₂O₁₇ appears. This phase is seen as an-end product at particular compositions in some BiMeVO_x materials [15,27]. Thus, like most BiMeVO_x compounds, we were able to stabilize the most symmetric form by increasing the substitution rate.

The evolutions of the unit cell parameters and the volume as a function of the niobium and copper content are reported in Figure 2. The unit-cell parameters have been reproduced in terms of mean orthorhombic dimension ($a_m = 5.5 \text{ \AA}$, $b_m = 5.6 \text{ \AA}$ and $c_m = 15.3 \text{ \AA}$) [28] using the relations $a_m = c_\alpha \times \sin(\beta)/3$, $b_m = a_\alpha \times \sin(\beta)$, $c_m = b_\alpha$ and $a_m = \sqrt{2} (a_\gamma)$ [19].

Globally, it can be noticed that a and b parameters decrease, while c parameter increases with the substitution amount of Cu^{2+} and Nb^{5+} ions. The increase of the oxygen vacancies number with x affect mainly a and b parameters from the moment they preferentially go to the equatorial positions. In fact, the substitution of Cu^{2+} and Nb^{5+} is accompanied correlatively by the increase of the dopant size, the effective ionic radius Cu^{2+} (0.74Å) and Nb^{5+} (0.64Å) compared with V^{5+} (0.54Å) [29], and the decrease of the oxide content ($-3x/4$ oxide ions). However, it appears clearly that volume of the unit-cell is more affected by the increase of the substituent size rather than the oxygen vacancies. This behavior, was already observed almost in all the Aurivillius family and particularly in BiMeVO_x materials [30]

Differential thermal analysis (DTA) of the $\text{Bi}_4\text{V}_{2-x}\text{Cu}_{x/2}\text{Nb}_{x/2}\text{O}_{11-3x/4}$ phases are represented in Figure 3. The existence of two endothermic peaks at 440-450°C and 530-560°C in the DTA curves can be observed for the samples with $x = 0.0$ and $x = 0.1$, respectively attributed to the $\alpha \rightarrow \beta$ and $\beta \rightarrow \gamma$ transitions. However, no thermal effect has been detected for compounds with $0.2 \leq x \leq 0.5$, which confirms its tetragonal symmetry and is in agreement with the XRD results. However, a strong transition is observed for the sample with $x = 0.6$ around 545°C, which confirms the presence of $\text{Bi}_8\text{V}_2\text{O}_{17}$ as a secondary phase and agrees with the XRD. The $\text{Bi}_8\text{V}_2\text{O}_{17}$ undergoes a phase transition at around 550 °C [27].

3.2 FT-IR spectroscopy measurements

The transmission FT-IR spectra for samples with different compositions $0.10 \leq x \leq 0.50$ in the range of 4000 to 400 cm^{-1} are shown in figure 4. As previously reported for $\text{Bi}_4\text{V}_{2-x}\text{Al}_{x/2}\text{Cu}_{x/2}\text{O}_{11-\delta}$ [15], the presence of adsorbed water in the powder samples of BiCuNbVO_x is seen also in the present solid solution. This is highlighted by the appearance of the water band at 1629 cm^{-1} and at a broad band around 3400 cm^{-1} and 3440 cm^{-1} .

From the spectra of the parent compound, the bands at 512 cm^{-1} can be assigned to the vibration mode of bismuth layers ν (Bi-O) in the BiO_6 distorted octahedral units superimposed to the longitudinal stretching mode of V-O_A and deformation mode δ_{as} (O-V-O) in perovskite vanadate layers (O_A is oxygen atom in apical position in the perovskite-like layers). The band around 614 cm^{-1} can be attributed to the stretching vibrations of Bi-O bonds in BiO_6 octahedral units [31,32]. In addition, the bands around 771 cm^{-1} and 831 cm^{-1} has been assigned to the symmetric ν_s (V-O) and asymmetric ν_{as} (V-O) stretching. A strong band at 1052 cm^{-1} can be also observed and attributed to the vibration of isolated V=O vanadyl groups in the VO_5 trigonal bipyramidal units [15]. Moreover, both ν_s (V-O) and ν_{as} (V-O) bands are clearly defined indicating an ordered structure of that phase. However, when the rate of substitution increases the bands become more and more broad, which indicate an enhancement of the disorder in these compounds and subsequently the stabilization of the tetragonal structure. This result is in good agreement with the XRD patterns. In addition, it can be noticed in the FT-IR spectra that some bands move to low or to high frequencies, while others completely disappear from the spectrum as the case of the band at 1052 cm^{-1} observed in the parent compound for instance [30,33]. The band located at about 512 cm^{-1} in $\text{Bi}_4\text{V}_2\text{O}_{11}$ spectrum, shifts towards the low frequencies as x increases. In fact, the size of the doping cation affects both V-O and Bi-O units, since the Bi^{3+} in (Bi_2O_2) layer forms weak bond with the perovskite slabs specially with oxygen apical. This special link, leads to a kind of dependency in the vibrations of the V-O and the Bi-O units. The same behavior had been observed in the $\text{Bi}_4\text{V}_{2-x}\text{Cu}_{x/2}\text{Al}_{x/2}\text{O}_{11-\delta}$ system [15]. In addition, we can observe a change in the width at half maximum of the band situated around 500 cm^{-1} in the FT-IR spectra of substituted phases. This change indicates that the oxygen environment could be modified during substitution and specially the O_A atoms, if it is supposed that this band is assigned to the Bi-O_A/V-O_A vibrations.

3.3 Raman spectroscopy

The room temperature Raman spectra of α and γ -BiCuNbVO_x compounds are shown in Figure 5. The main Raman bands of the studied BiCuNbVO_x with different compositions are observed in the 600 to 900 cm⁻¹ region and are attributed to the symmetrical and asymmetric stretching vibrations of V-O bonds in the VO₄ polyhedra [34].

It is important to note that, in the case of the parent compound (x=0), the band appearing beyond 920 cm⁻¹ is clearly visible in the Raman spectra. However, it disappears when the rate of substitution exceeds 0.1, domain where the tetragonal form is stabilized. The same behavior was also reported in previous works in the literature [34,35].

In order to estimate the V-O bond length, R (Å), from the Raman spectra 600–1000 cm⁻¹ frequency range, the empirical equation established by Hardcastle and Wachs [36] has been used. This relation can be written as:

$$\nu = 21349 \times \exp(-1.9176 \times R) \quad \text{Equation (1)}$$

when ν is the Raman shift of main band. The V-O bond lengths calculated from the previous equation are shown in Table 1. For the compositions $x < 0.2$, the values of the bond length (1.6813 Å) are slightly different from those of the parent compound (1.6801 Å). However, the values obtained for the tetragonal stabilized compounds ($x \geq 0.20$) are quite different from those of the Bi₄V₂O₁₁, which means that there are considerable changes in the local surrounding of the V cation in the perovskite slabs induced by the substitution of Cu/Nb.

Furthermore, both R and a parameter decrease with the increase of the rate of substitution. This indicates that the band used in Equation (1) could be attributed to V-O_e bond (O_e is oxygen atom in equatorial position in the perovskite-like layers), since the oxygen vacancies go preferentially to the equatorial positions.

3.4 Dilatometric study and characterization of the microstructure

The composition dependence of the shrinkage for Bi₄V_{2-x}Cu_{x/2}Nb_{x/2}O_{11-3x/4} ceramics ($0.0 \leq x \leq 0.5$) sintered at 800°C for 10 h under air is reported in Figure 6. The shrinkage values are almost constant for the ceramics with $x \leq 0.4$ (~5.4%). The densification becomes significant when $x > 0.4$, and an increase in the shrinkage of around 24% is observed for the ceramic with $x = 0.5$ (~6.7%). The increase of the anionic vacancies rate in the network seems to affect positively the densification mechanism of the ceramic.

The SEM micrographs of typical composition of the Bi₄V_{2-x}Cu_{x/2}Nb_{x/2}O_{11-3x/4} are presented in Figure 7. It can be clearly observed that when $x < 0.4$ the grains are not uniform and present residual porosity, largely along grain boundaries with almost unchanged size. However, when x exceeds 0.4, an important grain growth is observed accompanied with the appearance of micro-cracks. These microcracks could be resulted from the anisotropy of the BiMeVO_x materials, which may grow faster along certain crystallographic planes [13,37]. Beyond a critical size of the grains, the strong stresses could be created, which leads to the appearance of these micro-cracks. A large particles size distribution can be observed for $x > 0.4$. The grain size varies approximately between 20 and 40 μm.

3.5 Ionic conductivity

Starting from EIS measurements, typical Nyquist diagrams for BiCuNbVO_x ($x = 0.2$ and $x = 0.4$) obtained for medium temperature ($T = 300^\circ\text{C}$) are reported on Figure 8. A single broad semicircle lies from high frequencies to the intermediate ones can be seen, which means that the bulk and grain-boundaries contribution are not clearly deconvoluted. As waited, the straight line observed at low frequencies corresponds to the electrode polarization behavior [10,15].

The Arrhenius plots of total ceramic conductivity for the studied BiCuNbVO_x obtained between 120 and 720°C are reported in Figure 9. For materials with $x = 0$ and 0.1, the curves present two discontinuity assigned to the $\alpha \rightarrow \beta$ and $\beta \rightarrow \gamma$ transitions. However, those of the samples with tetragonal symmetry present only one discontinuity less or more pronounced depending on the rate of substitution. These transitions could be attributed to $\gamma \rightarrow \gamma'$ transformation. Therefore, the low temperature form in all the samples with tetragonal symmetry is not a γ polymorph but a γ' one, characterized by a relatively high activation energy (between 0.6 to 0.9 eV) and less conductive than γ polymorph (see Table 2). Furthermore, the compound with $x = 0.2$ presents the highest conductivity at low temperature. This compound contains the lowest concentration of dopant with a tetragonal structure. This behavior has been reported in many previous works and seems to be one of the characteristics of the BiMeVO_x materials [15]. However, at high temperature, the sample with $x = 0.1$ is more conductive than the sample with $x = 0.2$.

Beyond $x = 0.2$, a decrease in the ionic conductivity as the rate of substitution increases is observed. This phenomenon, commonly mentioned in BiMeVO_x materials, is assigned to the trap of the anion vacancies at the dopants, which introduce a trapping energy effect in the activation energy beside the motional enthalpy ΔH_m [38].

4. Conclusion

The simultaneous substitution of the parent phase Bi₄V₂O₁₁ with Cu²⁺ and Nb⁵⁺ allows the preparation of a family of single-phase compounds with the formula Bi₄V_{2-x}Cu_{x/2}Nb_{x/2}O_{11-3x/4} ($0.0 \leq x \leq 0.5$). The high temperature tetragonal form is stabilized between 0.2 and 0.5. However, it is not the γ form, but the more ordered and less conductive γ' .

The results obtained by FT-IR and Raman spectroscopy, which agree with the evolution of the cell parameters, could be explained by the distribution of the oxygen vacancies on apical or equatorial positions.

The microstructure of the prepared ceramics depends on the rate of substitution and becomes denser with increasing x . An important grain growth has also been observed when x increases and micro-cracks are observed in the ceramics with $x = 0.5$.

The electrical conductivity of the materials decreases when the rate of substitution increases in the γ form. The highest value has been obtained when 10% of vanadium had been substituted with copper and niobium ($x = 0.2$). Compared to the parent compounds Bi₄V₂O₁₁, the electrical conductivity of doubly substituted phases Bi₄V_{2-x}Cu_{x/2}Nb_{x/2}O_{11-3x/4} is improved. However, compared to mono-substituted phases Bi₄V_{1.8}Cu_{0.2}O_{10.7} ($\sigma \approx 4 \times 10^{-2} \text{ S.cm}^{-1}$ at 600°C), Bi₄V_{1.7}Nb_{0.2}O₁₁ ($\sigma \approx 2.5 \times 10^{-2} \text{ S.cm}^{-1}$ at 550°C), the values of electrical conductivity of doubly substituted phases Bi₄V_{1.8}Cu_{0.1}Nb_{0.1}O_{10.925} ($\sigma = 5.76 \times 10^{-3} \text{ S.cm}^{-1}$ at 600°C) had not improved but they are nearly of the same order of magnitude.

Acknowledgments

The authors are grateful to the Cadi Ayyad University Analysis and Characterization Center (CAC) for providing them with materials characterization techniques. They thank also ICMCB Bordeaux for Electrical conductivity measurements.

References

- [1] V.V.Kharton, F.M.B. Marques, A. Atkinson, Transport properties of solid oxide electrolyte ceramics: a brief review, *Solid State Ionics*, 174, 1–4 (2004) 135–149. <https://doi.org/10.1016/j.ssi.2004.06.015>
- [2] T. Kikuchi, A. Watanabe, K. Uchida, A family of mixed-layer type bismuth compounds, *Mater. Res. Bull.* 12 (1977) 299–304. [https://doi.org/10.1016/0025-5408\(77\)90148-9](https://doi.org/10.1016/0025-5408(77)90148-9).
- [3] A. Watanabe, M. Goto, Characterization of $\text{Bi}_2\text{W}_2\text{O}_9$ having a unique layered structure, *J. Less-Common Met.* 61 (1978) 265–272. [https://doi.org/10.1016/0022-5088\(78\)90222-9](https://doi.org/10.1016/0022-5088(78)90222-9).
- [4] I.H. Ismailzade, J. Ravez, $\text{Bi}_2\text{TiO}_4\text{F}_2$ – a new one-layer perovskite-like ferroelectric, *Ferroelectrics*. 21 (1978) 423–424. <https://doi.org/10.1080/00150197808237285>.
- [5] E.C. Subbarao, A family of ferroelectric bismuth compounds, *J. Phys. Chem. Solids*. 23 (1962) 665–676. [https://doi.org/10.1016/0022-3697\(62\)90526-7](https://doi.org/10.1016/0022-3697(62)90526-7).
- [6] C.K. Lee, M.P. Tan, A.R. West, Ge-doped bismuth vanadate solid electrolytes: synthesis, phase diagram and electrical properties, *J. Mater. Chem.*, 4 (1994) 525–528 <https://doi.org/10.1039/JM9940400525>
- [7] G. Mairesse, P. Roussel, R.N. Vannier, M. Anne, G. Nowogrocki, Crystal structure determination of α -, β - and γ - $\text{Bi}_4\text{V}_2\text{O}_{11}$ polymorphs. Part II: crystal structure of α - $\text{Bi}_4\text{V}_2\text{O}_{11}$, *Solid State Sci.* 5 (2003) 861–869. [https://doi.org/10.1016/S1293-2558\(03\)00016-5](https://doi.org/10.1016/S1293-2558(03)00016-5).
- [8] G. Mairesse, P. Roussel, R.N. Vannier, M. Anne, C. Pirovano, G. Nowogrocki, Crystal structure determination of α , β and γ - $\text{Bi}_4\text{V}_2\text{O}_{11}$ polymorphs. Part I: γ and β - $\text{Bi}_4\text{V}_2\text{O}_{11}$, *Solid State Sci.* 5 (2003) 851–859. [https://doi.org/10.1016/S1293-2558\(03\)00015-3](https://doi.org/10.1016/S1293-2558(03)00015-3).
- [9] F. Abraham, M.F. Debrouille-Gresse, G. Mairesse, G. Nowogrocki, Phase transitions and ionic conductivity in $\text{Bi}_4\text{V}_2\text{O}_{11}$ an oxide with a layered structure, *Solid State Ionics*. 28–30 (1988) 529–532. [https://doi.org/10.1016/S0167-2738\(88\)80096-1](https://doi.org/10.1016/S0167-2738(88)80096-1).
- [10] M. Alga, A. Ammar, B. Tanouti, A. Outzourhit, F. Mauvy, R. Decourt, Effect of Niobium doping on structural, thermal, sintering and electrical properties of $\text{Bi}_4\text{V}_{1.8}\text{Cu}_{0.2}\text{O}_{10.7}$, *J. Solid State Chem.* 178 (2005) 2873–2879. <https://doi.org/10.1016/j.jssc.2005.06.030>.
- [11] M. Alga, M. Wahbi, A. Ammar, B. Tanouti, J.C. Grenier, J.M. Reau, On new mixed conductors of $\text{Bi}_4\text{V}_{2-x}\text{Mn}_x\text{O}_{11-\delta}$ formulation, *J. Alloys Compd.* 256 (1997) 234–243. [https://doi.org/10.1016/S0925-8388\(96\)03106-4](https://doi.org/10.1016/S0925-8388(96)03106-4).
- [12] M. Alga, A. Ammar, R. Essalim, B. Tanouti, F. Mauvy, R. Decourt, Synthesis, sintering and electrical properties of P-doped $\text{Bi}_4\text{V}_2\text{O}_{11}$ ceramics, *Solid State Sci.* 7 (2005) 1173–1179. <https://doi.org/10.1016/j.solidstatesciences.2005.06.011>.
- [13] M. Alga, A. Ammar, R. Essalim, B. Tanouti, A. Outzourhit, F. Mauvy, R. Decourt, Study on structural, thermal, sintering and conductivity of Cu-Co doubly substituted $\text{Bi}_4\text{V}_2\text{O}_{11}$, *Ionics (Kiel)*. 11 (2005) 81–86. <https://doi.org/10.1007/BF02430405>.
- [14] R. Essalim, A. Ammar, B. Tanouti, F. Mauvy, Synthesis, thermal and electrical properties of Al-doped $\text{Bi}_4\text{V}_{1.8}\text{Cu}_{0.2}\text{O}_{10.7}$, *J. Solid State Chem.* 240 (2016) 122–125. <https://doi.org/10.1016/j.jssc.2016.05.026>.
- [15] R. Essalim, A. Ammar, M. Zamama, F. Mauvy, A study on structural properties, conductivity and FT-IR spectroscopy of Cu–Al doubly substituted $\text{Bi}_4\text{V}_2\text{O}_{11}$, *J. Solid State Chem.* 288 (2020) 121405. <https://doi.org/10.1016/j.jssc.2020.121405>.
- [16] R. Essalim, B. Tanouti, J.-P. Bonnet, J.M. Réau, Elaboration and electrical properties of ($0.20 \leq x \leq 0.55$) ceramics with the γ - $\text{Bi}_4\text{V}_2\text{O}_{11}$ type structure, *Mater. Lett.* 13 (1992) 382–386. [https://doi.org/10.1016/0167-577X\(92\)90073-S](https://doi.org/10.1016/0167-577X(92)90073-S).
- [17] Y. Yue, A. Dziegielewska, F. Krok, R.M. Whiteley, H. Toms, M. Malys, H. Yan, I. Abrahams, Local Structure and Conductivity in the BIGAVOX System, *J. Phys. Chem. C*. 126 (2022) 2108–2120. <https://doi.org/10.1021/acs.jpcc.1c08825>.

- [18] M. Malys, I. Abrahams, F. Krok, W. Wrobel, J.R. Dygas, The appearance of an orthorhombic BIMEVOX phase in the system $\text{Bi}_2\text{Mg}_x\text{V}_{1-x}\text{O}_{5.5-3x/2-\delta}$ at high values of x , *Solid State Ionics*. 179 (2008) 82–87. <https://doi.org/10.1016/j.ssi.2007.12.062>.
- [19] A. Dziegielewska, M. Malys, W. Wrobel, S. Hull, Y. Yue, F. Krok, I. Abrahams, $\text{Bi}_2\text{V}_{1-x}(\text{Mg}_{0.25}\text{Cu}_{0.25}\text{Ni}_{0.25}\text{Zn}_{0.25})_x\text{O}_{5.5-3x/2}$: A high entropy dopant BIMEVOX, *Solid State Ionics*. 360 (2021) 115543. <https://doi.org/10.1016/j.ssi.2020.115543>.
- [20] M.H. Paydar, A.M. Hadian, G. Fafilek, Studies on preparation, characterisation and ion conductivity of TI-CU double substituted $\text{Bi}_4\text{V}_2\text{O}_{11}$, *J. Eur. Ceram. Soc.* 21 (2001) 1821–1824. [https://doi.org/10.1016/S0955-2219\(01\)00123-6](https://doi.org/10.1016/S0955-2219(01)00123-6).
- [21] M.H. Paydar, A.M. Hadian, G. Fafilek, Ionic conductivity and crystal structure relationships in Ti/Cu substituted $\text{Bi}_4\text{V}_2\text{O}_{11}$, *J. Mater. Sci.* 39 (2004) 1357–1361. <https://doi.org/10.1023/B:JMSC.0000013896.02030.9d>.
- [22] E. V. Velichko, Z.A. Mikhailovskaya, M. V. Morozova, E.S. Buyanova, Y. V. Emel'yanova, S.A. Petrova, V.M. Zhukovskii, Synthesis, region of existence, structural characteristics, and conductivity of BI(CR, FE)VOX solid solutions, *Russ. J. Electrochem.* 47 (2011) 563–568. <https://doi.org/10.1134/S1023193511050181>.
- [23] A. Agnaou, W. Mhaira, R. Essalim, A. Turino, A. Ammar, M. Zamama, M. Alga, F. Mauvy, Structural Study and Ionic Conductivity of $\text{Bi}_4\text{V}_{2-x}\text{Si}_{x/2}\text{P}_{x/2}\text{O}_{11-\Delta}$ ($0.0 \leq x \leq 0.5$) Compounds, *SSRN Electron. J.* 178 (2022) 405. <https://doi.org/10.2139/ssrn.4244514>.
- [24] R.N. Vannier, G. Mairesse, F. Abraham, G. Nowogrocki, Double substitutions in $\text{Bi}_4\text{V}_2\text{O}_{11}$, *Solid State Ionics*. 70–71 (1994) 248–252. [https://doi.org/10.1016/0167-2738\(94\)90318-2](https://doi.org/10.1016/0167-2738(94)90318-2).
- [25] O. Joubert, A. Jouanneaux, M. Ganne, R. Vannier, G. Mairesse, Solid phase synthesis and characterization of new BIMEVOX series: $\text{Bi}_4\text{V}_{2-x}\text{M}_x\text{O}_{11}$ ($\text{M}=\text{Sb}^{\text{V}}, \text{Nb}^{\text{V}}$), *Solid State Ionics*. 73 (1994) 309–318. [https://doi.org/10.1016/0167-2738\(94\)90049-3](https://doi.org/10.1016/0167-2738(94)90049-3).
- [26] F. Abraham, J.C. Boivin, G. Mairesse, G. Nowogrocki, The bimevox series: A new family of high performances oxide ion conductors, *Solid State Ionics*. 40–41 (1990) 934–937. [https://doi.org/10.1016/0167-2738\(90\)90157-M](https://doi.org/10.1016/0167-2738(90)90157-M).
- [27] I. Abrahams, A. Kozanecka-Szmigiel, F. Krok, W. Wrobel, S.C.M. Chan M. , J.R. Dygas, Correlation of defect structure and ionic conductivity in δ -phase solid solutions in the Bi_3NbO_7 - Bi_3YO_6 system, *Solid State Ionics*, 177, 19-25 (2006)1761-1765. <https://doi.org/10.1016/j.ssi.2006.01.036>
- [28] G.N. Subbanna, L. Ganapathi, High resolution electron microscopy of bismuth oxides with perovskite layers, *Bull. Mater. Sci.* 9 (1987) 29–35. <https://doi.org/10.1007/BF02744390>.
- [29] R.D. Shannon, Revised effective ionic radii and systematic studies of interatomic distances in halides and chalcogenides, *Acta Crystallogr. Sect. A.* 32 (1976) 751–767. <https://doi.org/10.1107/S0567739476001551>.
- [30] D. Tripathy, A. Pandey, Structural and impedance studies of Ti^{IV} and Nb^{V} co-doped bismuth vanadate system, *J. Alloys Compd.* 737 (2018) 136–143. <https://doi.org/10.1016/j.jallcom.2017.12.079>.
- [31] R. Punia, R.S. Kundu, J. Hooda, S. Dhankhar, S. Dahiya, N. Kishore, Effect of Bi_2O_3 on structural, optical, and other physical properties of semiconducting zinc vanadate glasses, *J. Appl. Phys.* 110 (2011) 1–7. <https://doi.org/10.1063/1.3621188>.
- [32] R. Kaur, S. Thakur, K. Singh, Effect of two different sites substitution on structural and optical properties of $\text{Bi}_4\text{V}_2\text{O}_{11-\delta}$, *Phys. B Condens. Matter.* 440 (2014) 78–82. <https://doi.org/10.1016/j.physb.2014.01.032>.
- [33] D. Tripathy, A. Saikia, G.T. Tado, A. Pandey, Role of Al and Ti doping in modulating electrical properties of BIVOX system, *J. Adv. Ceram.* 8 (2019) 489–499. <https://doi.org/10.1007/s40145-019-0329-1>.
- [34] K. Trzciński, A. Borowska-Centkowska, M. Sawczak, A. Lisowska-Oleksiak, Photoelectrochemical properties of BIMEVOX (ME=Cu, Zn, Mn) electrodes in contact with

- aqueous electrolyte, *Solid State Ionics*. 271 (2015) 63–68. <https://doi.org/10.1016/j.ssi.2014.10.008>.
- [35] D. Tripathy, A. Pandey, Studies on structural and optical properties and its correlation with the ionic conductivity of the $\text{Bi}_2\text{VO}_{5.5}$ – based oxide ionic conductors, *Solid State Ionics*. 341 (2019) 115038. <https://doi.org/10.1016/j.ssi.2019.115038>.
- [36] F.D. Hardcastle, I.E. Wachs, Determination of molybdenum–oxygen bond distances and bond orders by Raman spectroscopy, *J. Raman Spectrosc.* 21 (1990) 683–691. <https://doi.org/10.1002/jrs.1250211009>.
- [37] M.C. Steil, J. Fouletier, M. Kleitz, P. Labrune, BICOVOX: Sintering and grain size dependence of the electrical properties, *J. Eur. Ceram. Soc.* 19 (1999) 815–818. [https://doi.org/10.1016/s0955-2219\(98\)00322-7](https://doi.org/10.1016/s0955-2219(98)00322-7).
- [38] J.A. Kilner, R.J. Brook, A study of oxygen ion conductivity in doped non-stoichiometric oxides, *Solid State Ionics*. 6 (1982) 237–252. [https://doi.org/10.1016/0167-2738\(82\)90045-5](https://doi.org/10.1016/0167-2738(82)90045-5).

x	ν (cm ⁻¹)	R (Å)
0.0	851.48	1.6801
0.1	849.52	1.6813
0.2	829.41	1.6938
0.3	852.48	1.6795
0.4	863.72	1.6726
0.5	866.10	1.6712

Table 1. The V-O bond distances estimated from Raman bands.

x	$\sigma_{300^\circ\text{C}}$ (S.cm ⁻¹)	$\sigma_{600^\circ\text{C}}$ (S.cm ⁻¹)	Ea _{LT} (eV) [T > 600 K]	Ea _{HT} (eV) [T > 800 K]
0.0	7.83×10^{-8}	3.27×10^{-3}	1.40	0.72
0.1	2.15×10^{-5}	1.00×10^{-2}	0.99	0.71
0.2	5.29×10^{-5}	5.76×10^{-3}	0.79	0.41
0.3	2.77×10^{-5}	1.72×10^{-3}	0.59	0.34
0.4	2.85×10^{-6}	2.64×10^{-4}	0.67	0.51
0.5	4.62×10^{-7}	1.91×10^{-4}	0.98	0.68

Table 2. Ionic conductivity values and activation energy of the Bi₄V_{2-x}Cu_{x/2}Nb_{x/2}O_{11-3x/4} ceramics.

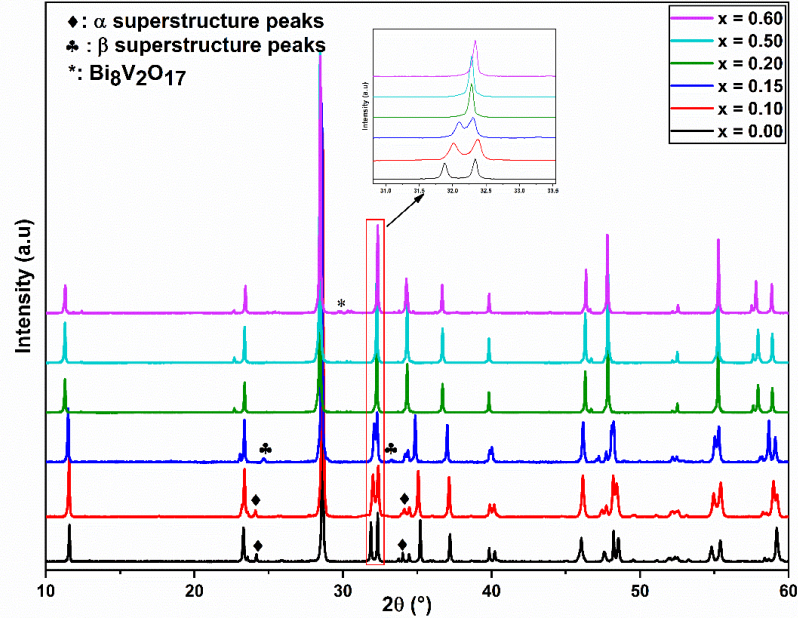


Fig 1. Powder XRD patterns of Bi₄V_{2-x}Cu_{x/2}Nb_{x/2}O_{11-3x/4} compounds with (x = 0 ; 0.1 ; 0.15 ; 0.2 ; 0.5 ; 0.6).

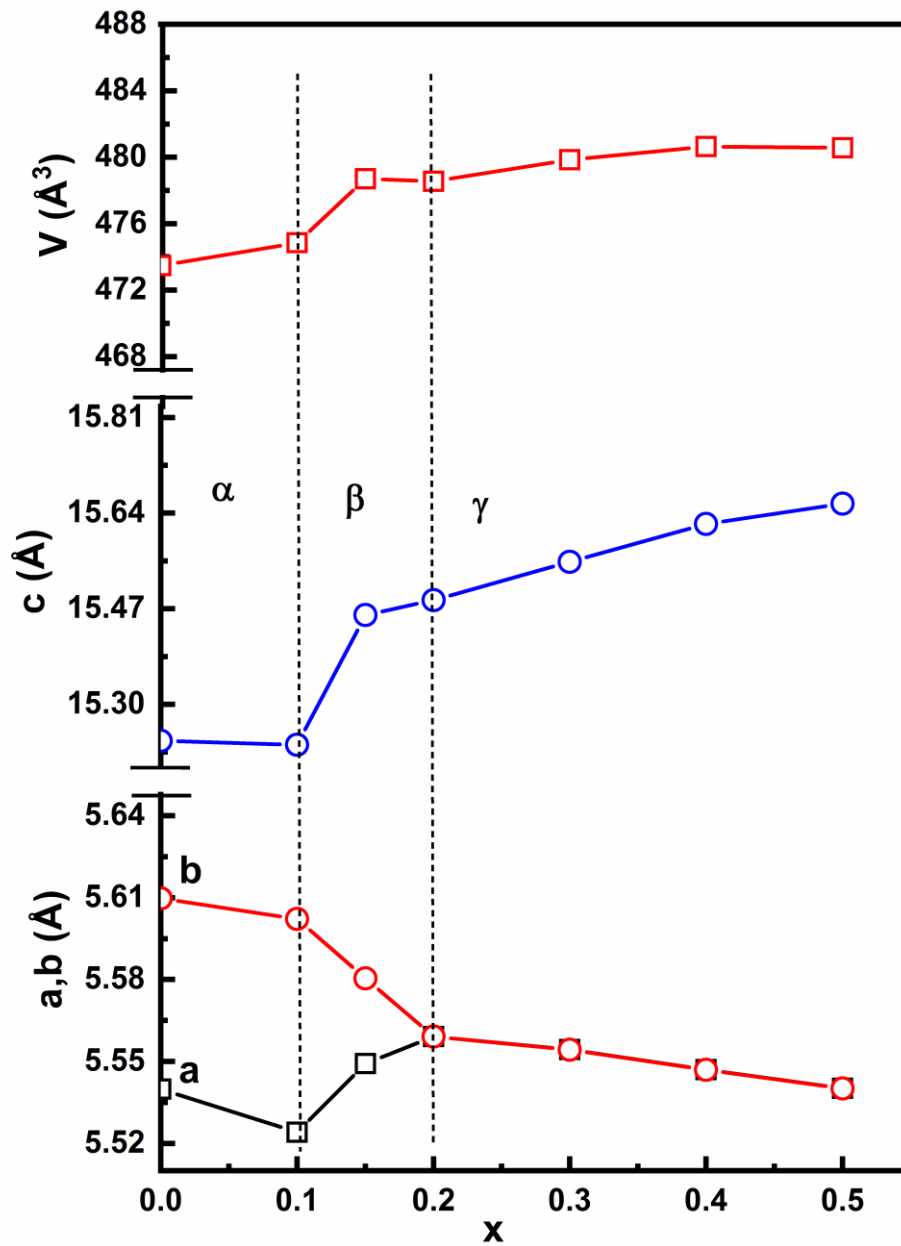


Fig 2. Evolution versus x of the unit cell parameters and the volume of $\text{Bi}_4\text{V}_{2-x}\text{Cu}_{x/2}\text{Nb}_{x/2}\text{O}_{11-3x/4}$.

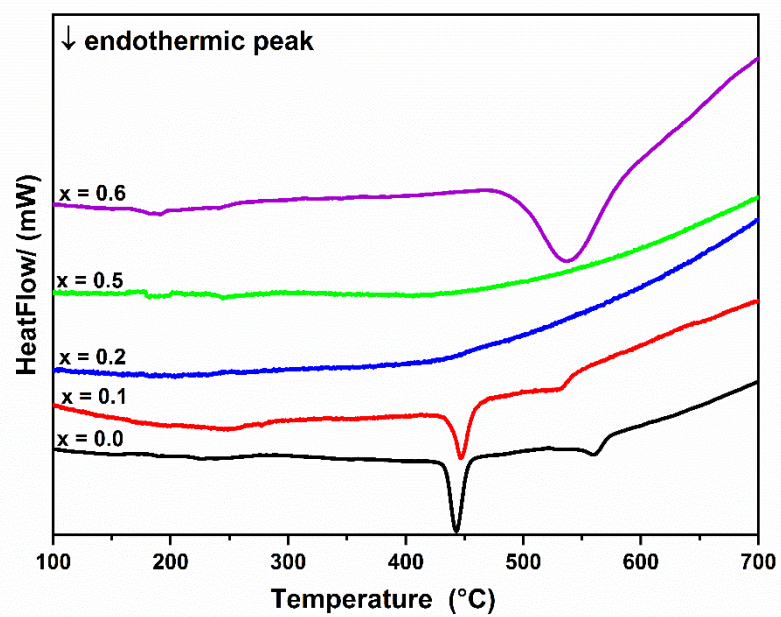


Fig 3.DTA curves of $\text{Bi}_4\text{V}_{2-x}\text{Cu}_{x/2}\text{Nb}_{x/2}\text{O}_{11-3x/4}$ solid solution.

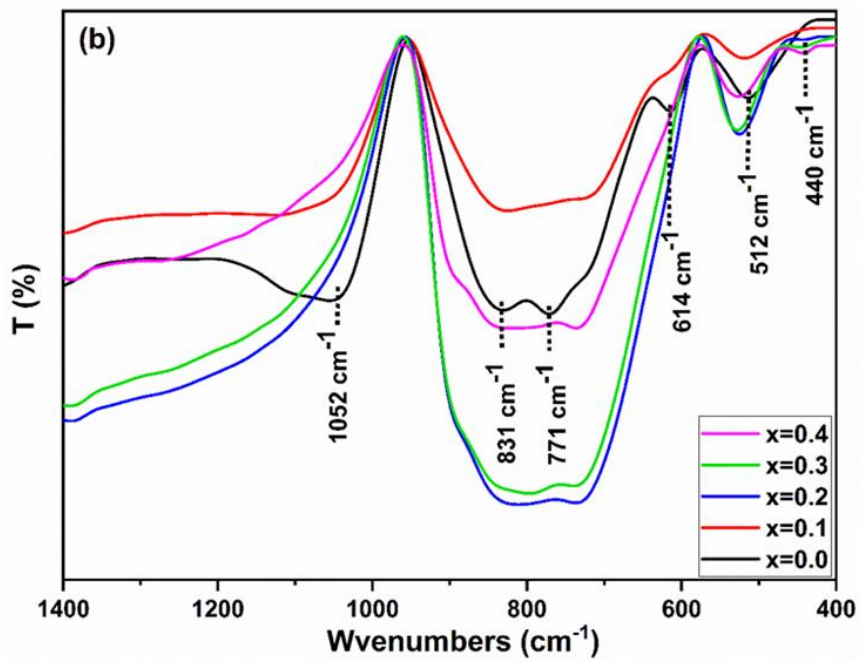
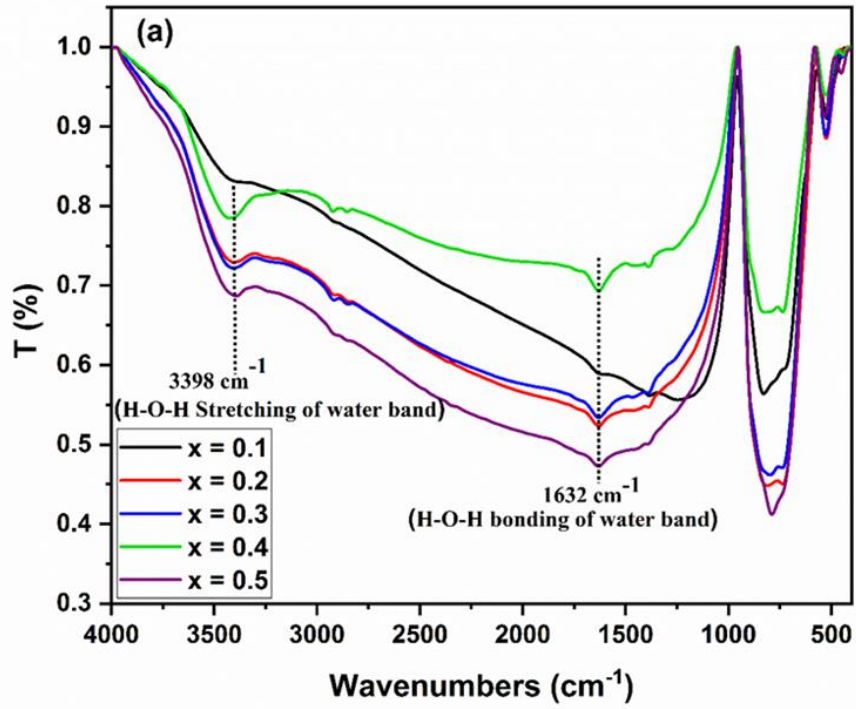


Fig 4. FT-IR spectra of $\text{Bi}_4\text{V}_{2-x}\text{Cu}_{x/2}\text{Nb}_{x/2}\text{O}_{11-3x/4}$ solid solution
 (a): (4000-400 cm^{-1}), (b): (1400-400 cm^{-1}).

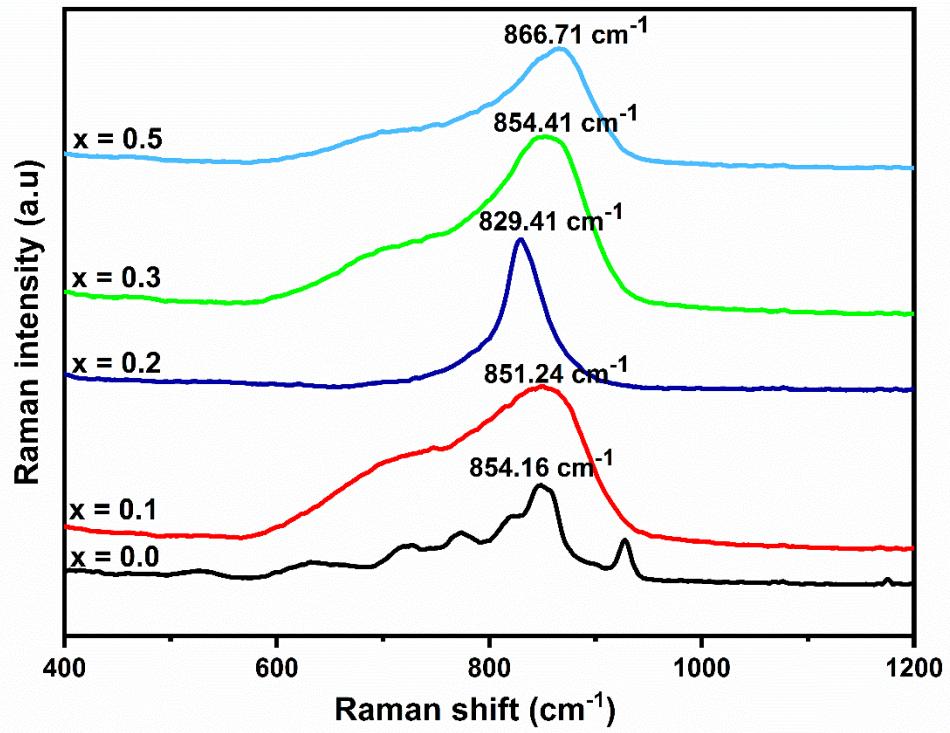


Fig 5. Raman spectra of $\text{Bi}_4\text{V}_{2-x}\text{Cu}_{x/2}\text{Nb}_{x/2}\text{O}_{11-3x/4}$ solid solution.

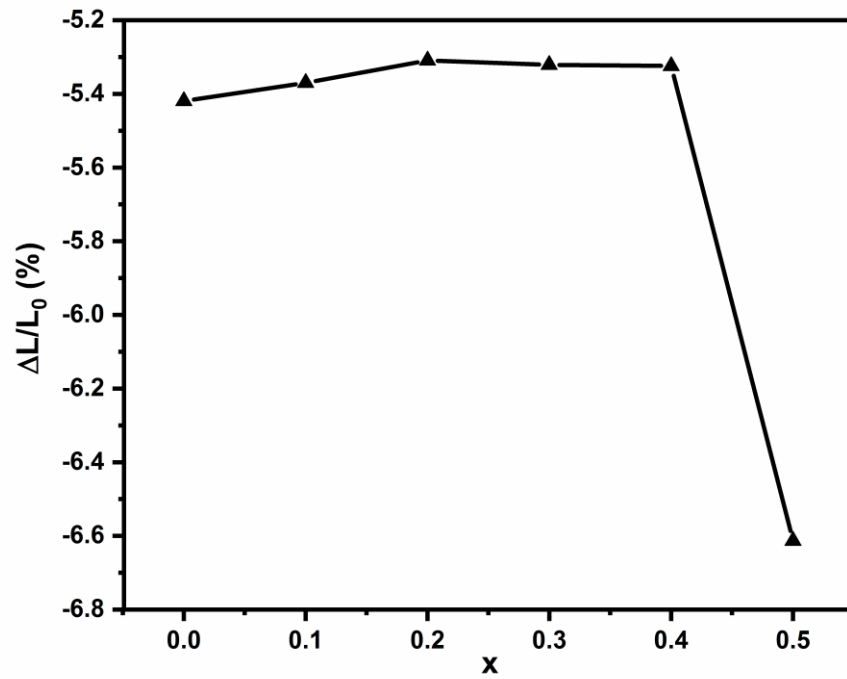


Fig 6. Composition dependence of the shrinkage of $\text{Bi}_4\text{V}_{2-x}\text{Cu}_{x/2}\text{Nb}_{x/2}\text{O}_{11-3x/4}$ solid solution.

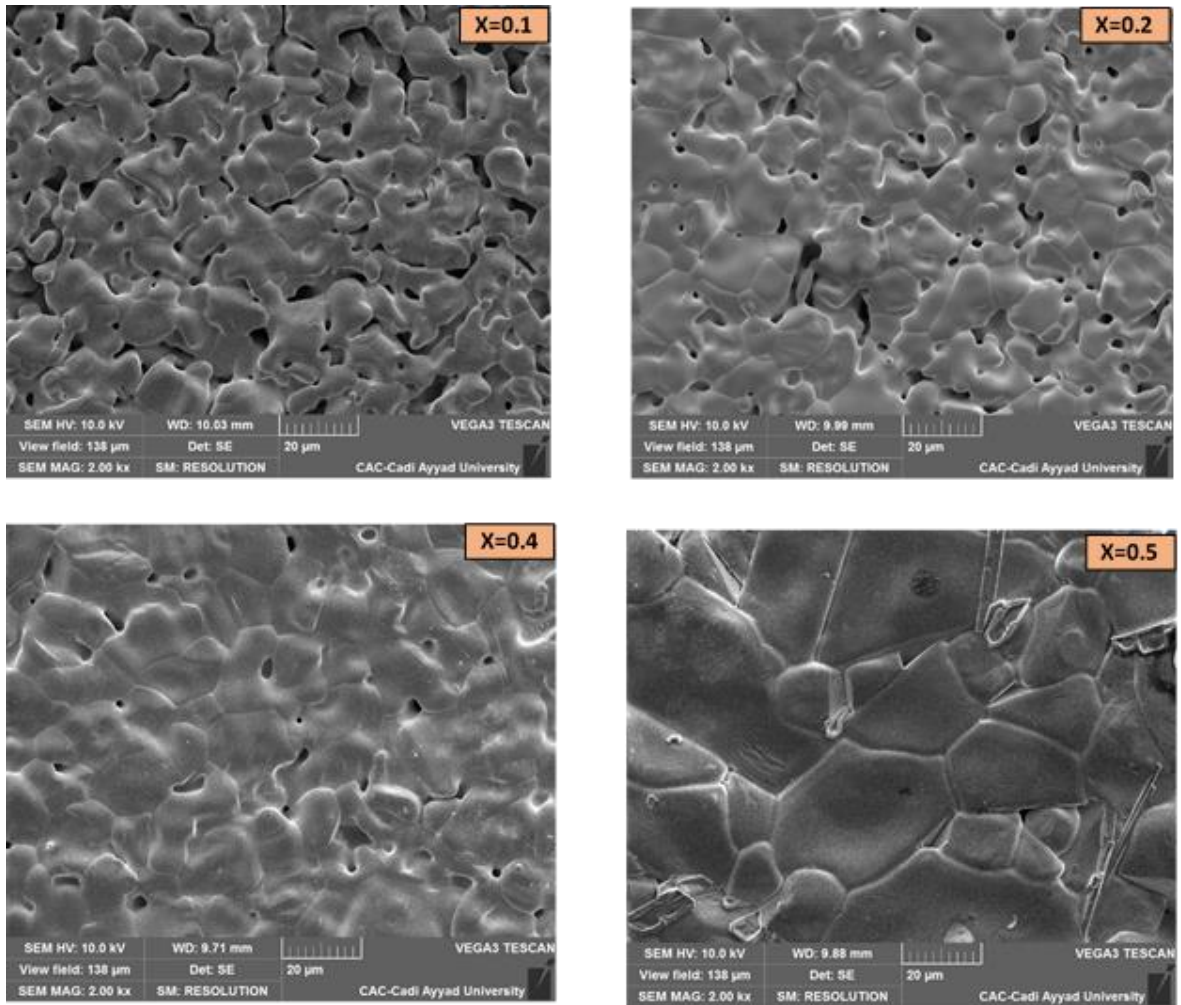


Fig 7. SEM micrographs of sintered $\text{Bi}_4\text{V}_{2-x}\text{Cu}_{x/2}\text{Nb}_{x/2}\text{O}_{11-3x/4}$ solid solution.

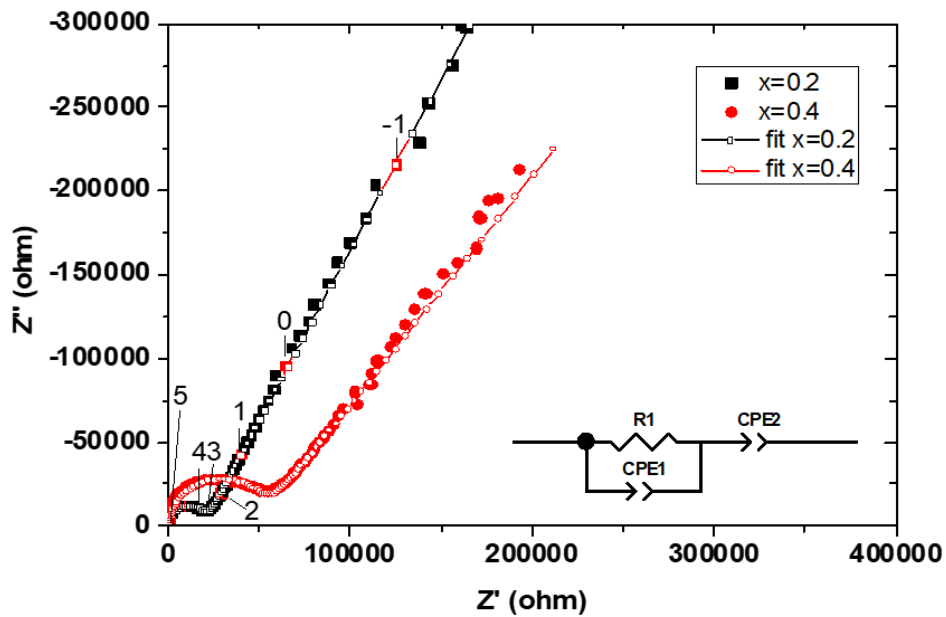


Fig 8. Nyquist plot and fit results for $\text{Bi}_4\text{V}_{2-x}\text{Cu}_{x/2}\text{Nb}_{x/2}\text{O}_{11-3x/4}$ sample with $x = 0.2$ and $x = 0.4$. The used Equivalent Circuit is inserted in the figure.

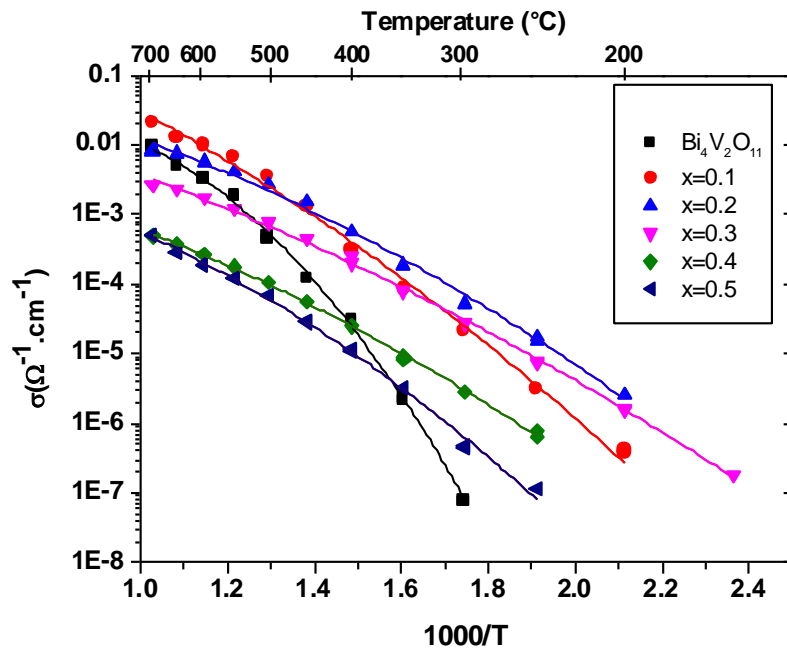


Fig 9. Arrhenius plots of the electrical conductivity of the $\text{Bi}_4\text{V}_{2-x}\text{Cu}_{x/2}\text{Nb}_{x/2}\text{O}_{11-3x/4}$ compounds.